Iraqi Journal of Science

ISSN: 0067-2904
GIF: 0.851

Elastic Electron Scattering Form Factors and Charge Densities for Some Nuclei in 2s-1d Shell Using the Effect of Occupation Numbers

Wasan Z. Majeed* , Arkan R. Ridha
Department of Physics, College of Science, University of Baghdad,Baghdad ,Iraq

Abstract

Elastic electron scattering form factors, charge density distributions and charge, neutron and matter root mean square (rms) radii for ^{24}Mg, ^{28}Si and ^{32}S nuclei are studied using the effect of occupation numbers. Single-particle radial wave functions of harmonic-oscillators (HO) potential are used. In general, the results of elastic charge form factors showed good agreement with experimental data. The occupation numbers are taken to reproduce the quantities mentioned above. The inclusion of occupation numbers enhances the form factors to become closer to the data. For the calculated charge density distributions, the results show good agreement with experimental data except the fail to produce the hump in the central region for ^{28}Si nucleus. Finally, the calculated charge rms radii for the nuclei under study show good agreement with experimental data.

PACS number(s): 21.60.Cs, 21.60.De, 25.30.Bf, 27.10.+h, 27.20.+n

Keywords: stable nuclei, shell model, charge density distribution, elastic charge form factor, rms charge, neutron, and matter radii.

عوامل التشكل للاستطارة الالكترونية المرنة وتوزيعات كثافة الشحنة لبعض النوى الواقعة في الغلاف 2s- 1d باستخدام تاثير اعداد الاشغال

وسن زهير ، اركان رفعه

قسم الفيزياء ، كلية العلوم ،جامعة بغداد ، بغداد ، العراق

الخلاصة

تمت دراسة توزيعات كثافة الشحنة للحالة الأرضية وعوامل التشكل للاستطارة المرنة بالإضافة إلى أنصاف الأقطارالشحنية والنيوترونية والكتلية للنوى ^{24}Mg, ^{28}Si and ^{32}S ، باستخدام اعداد الاشغال. تم استخدام االدوال الموجية القطرية لجهد المتذبذب التوافقي. بالنسبة لنتائج عوامل التشكل الشحنية المحسوبة باستخدام نموذج القشرة، اظهرت النتائج تطابق جيد مع النتائج العملية. حيث تبين ان استخدام تاثير اعداد الاشغال للمستويات المختلفة يجعل النتائج اقرب للقيم العملية. كما أظهرت النتائج تطابق جيد بين توزيعات الكثافة الشحنية المحسوبة والقيم العملية باستخدام نموذج القشرة ماعدا عدم التنبؤ بالسنام او القمة الموجودة في توزيعات الكثافة الشحنية لنواة ^{28}Si. اخيرا فيما يخص قيم انصاف الاقطار الشحنية المحسوبة فتم توليدها بنجاح لتطابق العملية المقابلة لها.

Introduction

The scattering of electrons from nuclei gives the most precise information about nuclear size and charge distribution, and it provides important information about the electromagnetic currents inside

*Email: wasan_zmz@yahoo.com

the nuclei. Electron scattering can provide a good test since it is sensitive to the spatial dependence of the charge and current densities [1].

The charge density distribution is one of the many most important quantities in the nuclear structure which has been well studied experimentally over a wide range of nuclei. This interest in charge density is related to the basic bulk nuclear characteristics such as the shape and size of nuclei, their binding energies, and other quantities which are connected with charge density distribution [2,3].

Many attempts made to explain the experimental data of electron scattering and to understand the nature of nuclear force and the structure of the nuclei. Several experimental and theoretical groups have devoted their works for studying the electron scattering from sd-shell nuclei [4-8].

In this work, the charge density distributions, elastic form factors and root mean square radii are studied for ^{24}Mg, ^{28}Si and ^{32}S nuclei using shell occupation numbers different from those predicted by simple shell model. This model have been determined which lead to a good description of the charge density and elastic form factor data. The single- particle radial wave functions of harmonic-oscillators (HO) potential are used to reproduce the corresponding experimental data.

Theoretical formulations

The transition charge density one-body operator of rank J for point nucleons (with isospin $t_z = 1/2$) or neutrons ($t_z = -1/2$) can be written as [9]:

$$\hat{\rho}_J = \sum_{k=1}^{A} e(t_z) \frac{\delta(r - r_k)}{r^2} Y_{J,M_J}(\Omega_{r_k}), \qquad (1)$$

where

$$e(t_z) = \frac{1 + 2t_z(k)}{2}.$$

In the above Eq. (1), $Y_{J,M_J}(\Omega_{r_k})$ and $\delta(\vec{r} - \vec{r}_k)$ are spherical harmonic and Dirac delta functions respectively. The multipolarity J of the transition is restricted by the following angular momentum and parity selection rules:

$\left|J_i \_ J_f\right| \le J \le J_i + J_f$

and

$\pi_i \pi_f = (-1)^J$ (for Coulomb transitions).

The reduced matrix element of the transition charge density operator of Eq. (1), can be written as [9]:

$$\left\langle J_f \left\| \hat{\rho}_J(\vec{r}) \right\| J_i \right\rangle = \frac{1}{\sqrt{4\pi(2J_i + 1)}} \sum_{ab} X_{a,b,t_z}^{J_f, J_i, J} \left\langle j_a \left\| Y_J \right\| j_b \right\rangle R_{n_a l_a}(r) R_{n_b l_b}(r), \qquad (2)$$

where a and b stand for the single-particle states and are specified by:

$\left|p\right\rangle = \left|n_p l_p\right\rangle \left| j_p m_p \right\rangle$, (the state p represents either a or b)

The states $\left|J_i\right\rangle$ and $\left|J_f\right\rangle$ are initial and final total angular momentum of the nuclei under study. In Eq. (2), $R_{n_p l_p}(r)$ is the radial part of the HO wave function, $\left\langle j_a \left\| Y_J \right\| j_b \right\rangle$ is the reduced matrix element of the spherical harmonic and $X_{a,b,t_z}^{J_f, J_i, J}$ is the proton ($t_z = 1/2$) or neutron ($t_z = -1/2$) one body density matrix element given by the second quantization as [9]:

$$X_{a,b,t_z}^{J_f, J_i, J} = \frac{\left\langle J_f \left\| \left[a_{a,t_z}^{+} \otimes \tilde{a}_{b,t_z} \right]^J \right\| J_i \right\rangle}{\sqrt{2J + 1}}. \qquad (3)$$

The relation between these triply reduced $X_{a,b,t_z,\Delta T}^{J_f, J_i, J}$ and the proton or neutron $X_{a,b,t_z}^{J_f, J_i, J}$ of Eq. (2) is given by [10]:

$$X^{J_f,J_i,J}_{a,b,t_z} = (-1)^{T_f-T_z}\sqrt{2}\begin{pmatrix} T_f & 0 & T_i \\ -T_z & 0 & T_z \end{pmatrix}\frac{X^{J_f,J_i,J}_{a,b,t_z,\Delta T=0}}{2} + 2t_z(-1)^{T_f-T_z}\sqrt{6}\begin{pmatrix} T_f & 1 & T_i \\ -T_z & 0 & T_z \end{pmatrix}\frac{X^{J_f,J_i,J}_{a,b,t_z,\Delta T=1}}{2} \quad (4)$$

where the triply reduced $X^{J_f,J_i,J}_{a,b,t_z,\Delta T}$ elements are given in the second quantization as:

$$X^{\Gamma_f,\Gamma_i,J}_{\alpha,\beta,\Delta T} = \frac{\left\langle \Gamma_f \left\| \left[a^+_\alpha \otimes \tilde{a}_\beta\right]^{J,\Delta T} \right\| \Gamma_i \right\rangle}{\sqrt{2J+1}\sqrt{2\Delta T+1}} \quad (5)$$

Here, Greek symbols are utilized to indicate quantum numbers in coordinate space and isospace (i.e., $\Gamma_i \equiv J_i T_i$ and $\Gamma_f \equiv J_f T_f$). The $X^{\Gamma_f,\Gamma_i,J}_{\alpha,\beta,\Delta T}$ elements contain all the information about transitions of given multipolarities which are embedded in the model wave functions.

For the ground state density distribution, one has $J_i = J_f$, $J = 0$ and $a = b$ (i.e., $n_a = n_b$, $l_a = l_b$ and $j_a = j_b$). Therefore, the reduced matrix element of the spherical harmonic presented in Eq. (2) will give the following result [11]:

$$\left\langle j_a \left\| Y_0 \right\| j_a \right\rangle = (-1)^{2j_a+1}\sqrt{\frac{2j_a+1}{4\pi}} = \sqrt{\frac{2j_a+1}{4\pi}} \quad (6)$$

Substituting Eq. (6) into Eq. (2), one finds that:

$$\rho_{t_z}(r) = \frac{1}{4\pi\sqrt{(2J_i+1)}}\sum_\alpha \sqrt{2j_a+1}\, X^{J_i,J_i,0}_{a,a,t_z}\left|R_{n_a l_a}(r,b_{t_Z})\right|^2 \quad (7)$$

Where

$\rho_{t_z}(r) = \left\langle J_i \left\| \hat{\rho}_J(\vec{r}) \right\| J_i \right\rangle$.

In Eq. (7), b_{t_Z} values are the HO size parameters of protons ($t_z = 1/2$)) and neutrons ($t_z = -1/2$)).

It is worth mentioning that the final formula in Eq. (7) is normalized to the atomic number (*Z*) (point proton density) and neutron number (*N*) (point neutron density) as follows:

$$4\pi\int_0^\infty \rho_{p\,or\,n}(r)r^2 dr = Z\ or\ N.$$

For pure configuration, $X^{J_i,J_i,0}_{a,a,t_z}$ can be written as:

$$X^{J_i,J_i,0}_{a,a,t_z} = \frac{\sqrt{2J_i+1}}{\sqrt{2j_a+1}}n_{a,t_Z}, \quad (8)$$

Where n_{a,t_Z}, represents the number of neutrons ($t_z = 1/2$) or protons ($t_z = -1/2$) in the subshells.

Finally, Eq. (7) can be simplified with the aid of result in Eq. (8) to the form:

$$\rho_{t_z}(r) = \frac{1}{4\pi}\sum_a n_{a,t_Z}\left|R_{n_a l_a}(r,b_{t_Z})\right|^2 \quad (9)$$

The charge density distribution $\rho_{ch}(r)$ is obtained by folding the proton density ρ_{pr} into the distribution of the point protons of Eq. (9) as follows [12]:

$$\rho_{ch}(\vec{r}) = \int \rho_p(\vec{r})\rho_{pr}(\vec{r}-\vec{r}')d\vec{r}' \quad (10)$$

Where ρ_{pr} takes the Gaussian form as [12]:

$$\rho_{pr}(r)=\frac{1}{\left(\sqrt{\pi}a_{pr}\right)^3}e^{\left(\frac{-r^2}{a_{pr}^2}\right)} \quad (11)$$

Where $a_{pr}=0.65\ fm$. Such value of a_{pr} produces the experimental charge rms radius of proton, $\langle r\rangle_{pr}^{\frac{1}{2}}=\left(\frac{3}{2}\right)^{1/2}a_{pr}\approx 0.8\ fm$.

The charge rms radii of can be directly deduced from their density distributions as follows [12]:

$$\langle r\rangle_{ch}^{\frac{1}{2}}=\sqrt{\frac{4\pi}{Z}\int_0^\infty \rho_{ch}(r)r^2dr} \quad (12)$$

In plane wave Born approximation (PWBA) the elastic charge form factors are Fourier transform to their corresponding ground charge density distribution [12]:

$$F_{ch}(q)=\frac{4\pi}{qZ}\left[\int_0^\infty \rho_p(r)\sin(qr)rdr\right]f_{fc}(q)\,f_{cm}(q) \quad (13)$$

Where $f_{fc}(q)$ and $f_{cm}(q)$ are free nucleon form factor and center of mass correction, respectively, given by [12]:

$$f_{fc}(q)=e^{\left(\frac{-0.43q^2}{4}\right)} \quad (14)$$

and

$$f_{cm}(q)=e^{\left(\frac{b_p^2q^2}{4A}\right)} \quad (15)$$

Where *A* in Eq. (15) represents the mass number of the nucleus under study.

It is worth mentioning that $F_{ch}(q)$ in Eq. (13) is normalized to unity in the limit $q\to 0$.

Results and discussion:

In this work, the charge density distributions, charge rms radii and elastic charge form factors are calculated in shell model using single-particle radial wave functions of harmonic-oscillators (HO) potential. The present calculations take two methods: the first uses occupation numbers as predicted by simple shell model; such calculations are denoted by SSM. The second method uses occupation numbers different from those predicted by SSM and controlled to reproduce the calculated charge density distributions, charge rms radii and elastic charge form factors to fit experimental data, such method is denoted by MSM (modified shell model).

For ^{24}Mg nucleus, the HO size parameter is taken to be $b=1.62\ fm$ to reproduce best match with experimental charge density distribution and form factor. The occupation numbers in SSM and MSM are tabulated in Table -1 and -2, respectively.

Table 1- The calculated $X_{a,a,t_z}^{J_i,J_i,0}$ for ^{24}Mg for neutrons and protons calculated in SSM method.

State 1	State 2	Number of protons ($n_{a,p}$) and neutrons ($n_{a,n}$)	$X_{a,a,t_z}^{J_i,J_i,0}$
$1s_{1/2}$	$1s_{1/2}$	2.0	1.414214
$1p_{3/2}$	$1p_{3/2}$	4.0	2.0
$1p_{1/2}$	$1p_{1/2}$	2.0	1.414214
$1d_{5/2}$	$1d_{5/2}$	4.0	1.632993

Table 2- The calculated $X_{a,a,t_z}^{J_i,J_i,0}$ for ^{24}Mg for neutrons and protons calculated in MSM method.

State 1	State 2	Number of protons ($n_{a,p}$) and neutrons ($n_{a,n}$)	$X_{a,a,t_z}^{J_i,J_i,0}$
$1s_{1/2}$	$1s_{1/2}$	0.85	0.601041
$1p_{3/2}$	$1p_{3/2}$	3.1	1.55000
$1p_{1/2}$	$1p_{1/2}$	1.5	1.060660
$1d_{5/2}$	$1d_{5/2}$	1.3	0.530723
$1d_{3/2}$	$1d_{3/2}$	0.0	0.0
$2s_{1/2}$	$2s_{1/2}$	0.4	0.282843
$1f_{7/2}$	$1f_{7/2}$	4.85	1.714734
$1f_{5/2}$	$1f_{5/2}$	0.0	0.0

The calculated charge density distributions in SSM and MSM are displayed in Figure-1 by dashed and solid curves, respectively. It's clear from Fig. (1), that the result of the solid curve (MSM) is better than the calculation of dashed curve (SSM). This support the idea of the existence of strong mixing configuration between 1s and 1f shells according to $X_{a,a,t_z}^{J_i,J_i,0}$ suggested in Table 2.

In Figure -2, the calculated elastic charge form factors are displayed by dashed and solid curves calculated in SSM and MSM, respectively. The result of solid is better than the result of SSM. Although the match with experimental data at high q values is bad due to slight deviation in the calculated charge density distribution at central region (r < 2.5 fm) from experimental data, the result in general has good agreement with experiment.

In Table 3, the results of the calculated rms charge, neutron, and matter radii are tabulated. The results of the calculated charge rms radii in MSM are in excellent agreement with experimental data on contrary to the results of the SSM.

Table 3- The calculated rms charge, neutron, and matter radii of ^{24}Mg nucleus.

Technique	$\langle r \rangle_{ch}^{1/2}$ fm	Exp. $\langle r \rangle_{ch}^{1/2}$ fm [13]	$\langle r \rangle_{n}^{1/2}$ fm	$\langle r \rangle_{m}^{1/2}$ fm	Exp. $\langle r \rangle_{m}^{1/2}$ fm [14]
SSM	2.762	3.08(5)	2.645	2.645	2.79(15)
MSM	3.081		2.977	2.977	

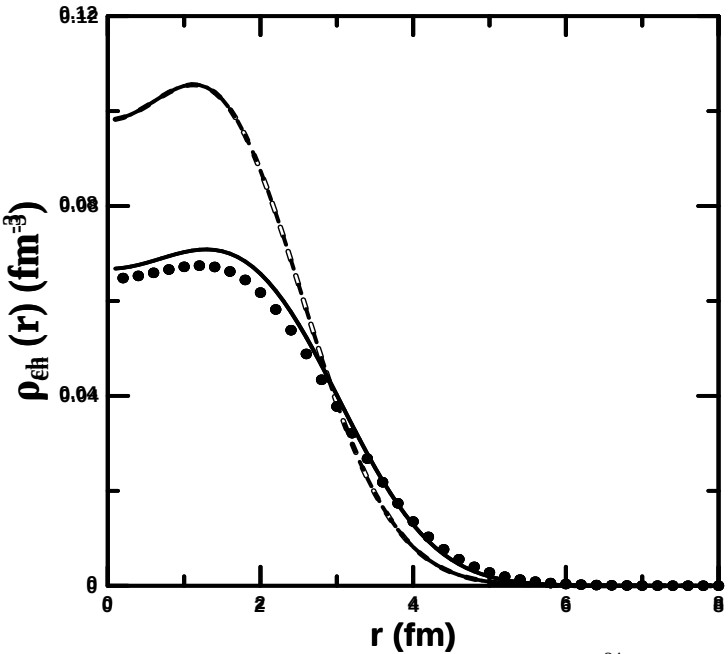

Figure 1- The calculated charge density distribution of ^{24}Mg nucleus. The dotted curve represents experimental data [13]. The dashed and solid curves are the calculated charge density using SSM and MSM methods, respectively.

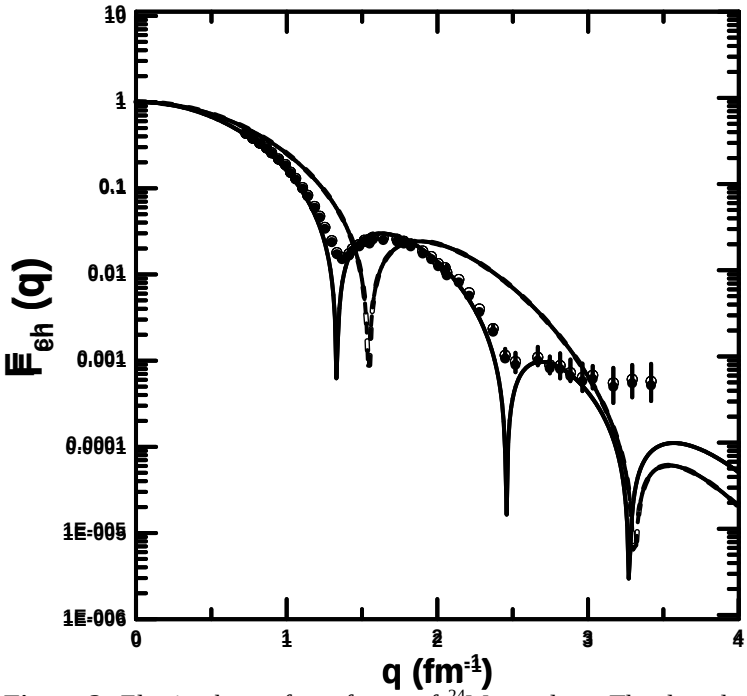

Figure 2- Elastic charge form factor of ^{24}Mg nucleus. The dotted curve represents experimental data [6]. The dashed and solid curves are the calculated charge form factors calculated using SSM and MSM methods, respectively.

For ^{28}Si nucleus, the values of the HO size parameter is taken to be $b = 1.63\ fm$ to reproduce best match with experimental charge density distribution and form factor. The occupation numbers in SSM and MSM are tabulated in Table -4 and 5, respectively. In Figure 3, the calculated charge density distributions in SSM and MSM are displayed by dashed and solid curves, respectively. The result of the solid curve has a good agreement with experimental data, but there is an overestimation in the calculation in the central region (r < 1.5 fm). This necessitates the importance of the existence of strong mixing configuration between 1s and 2p shells according to $X^{J_i,J_i,0}_{a,a,t_z}$ suggested in Table -5.

In figure -4, the results of the calculated elastic charge form factors are displayed by dashed and solid curves calculated in SSM and MSM, respectively. The result of solid curve has a very good agreement with experimental data for all *q* values.

The calculated charge, neutron, and matter rms radii are tabulated in Table -6. The results of the calculated charge rms radii in MSM are overestimated in comparison with experimental data due to the contribution coming from higher $1f_{7/2}$ subshell.

Table 4- The calculated $X^{J_i,J_i,0}_{a,a,t_z}$ for ^{28}Si for neutrons and protons calculated in SSM Method.

State 1	State 2	Number of protons ($n_{a,p}$) and neutrons ($n_{a,n}$)	$X^{J_i,J_i,0}_{a,a,t_z}$
$1s_{1/2}$	$1s_{1/2}$	2.0	1.414214
$1p_{3/2}$	$1p_{3/2}$	4.0	2.0
$1p_{1/2}$	$1p_{1/2}$	2.0	1.414214
$1d_{5/2}$	$1d_{5/2}$	6.0	2.449490

Table 5- The calculated $X_{a,a,t_z}^{J_i,J_i,0}$ for ^{28}Si for neutrons and protons calculated in MSM method.

State 1	State 2	Number of protons ($n_{a,p}$) and neutrons ($n_{a,n}$)	$X_{a,a,t_z}^{J_i,J_i,0}$
$1s_{1/2}$	$1s_{1/2}$	0.9	0.636396
$1p_{3/2}$	$1p_{3/2}$	3.0	1.50000
$1p_{1/2}$	$1p_{1/2}$	1.0	0.707107
$1d_{5/2}$	$1d_{5/2}$	4.0	1.632993
$1d_{3/2}$	$1d_{3/2}$	0.0	0.0
$2s_{1/2}$	$2s_{1/2}$	0.5	0.353553
$1f_{7/2}$	$1f_{7/2}$	4.2	1.484924
$1f_{5/2}$	$1f_{5/2}$	0.0	0.0
$2p_{3/2}$	$2p_{3/2}$	0.4	0.20000

Table 6: The calculated rms charge, neutron, and matter radii of ^{28}Si nucleus.

Technique	$\langle r \rangle_{ch}^{1/2}$ *fm*	Exp. $\langle r \rangle_{ch}^{1/2}$ *fm* [13]	$\langle r \rangle_{n}^{1/2}$ *fm*	$\langle r \rangle_{m}^{1/2}$ *fm*
SSM	2.834	3.106(30)	2.72	2.72
MSM	3.114		3.011	3.011

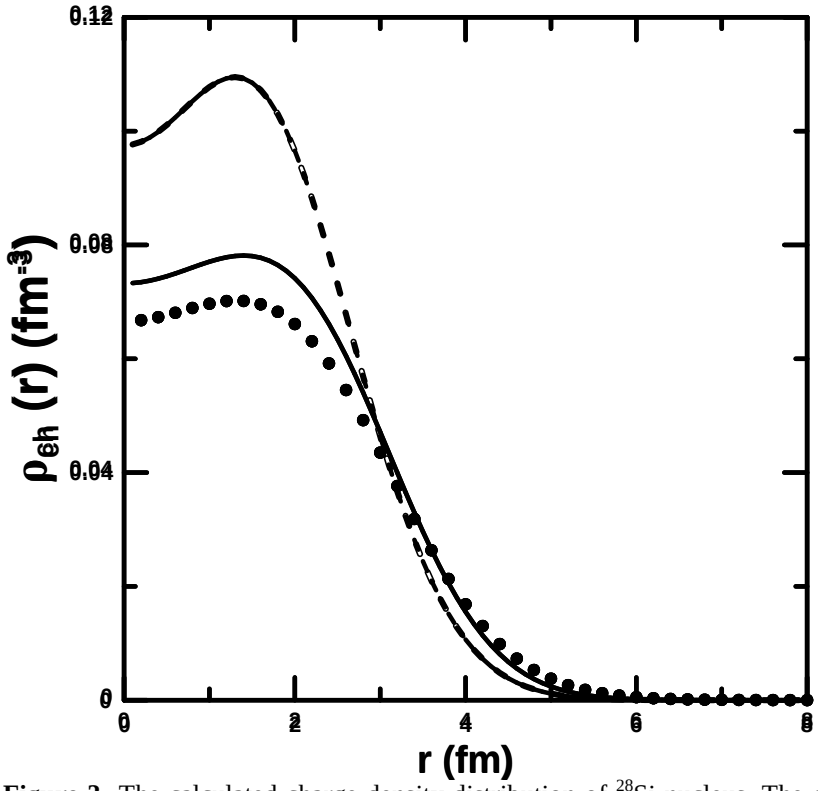

Figure 3- The calculated charge density distribution of ^{28}Si nucleus. The dotted curve represents experimental data [13]. The dashed and solid curves are the calculated charge density using SSM and MSM methods, respectively.

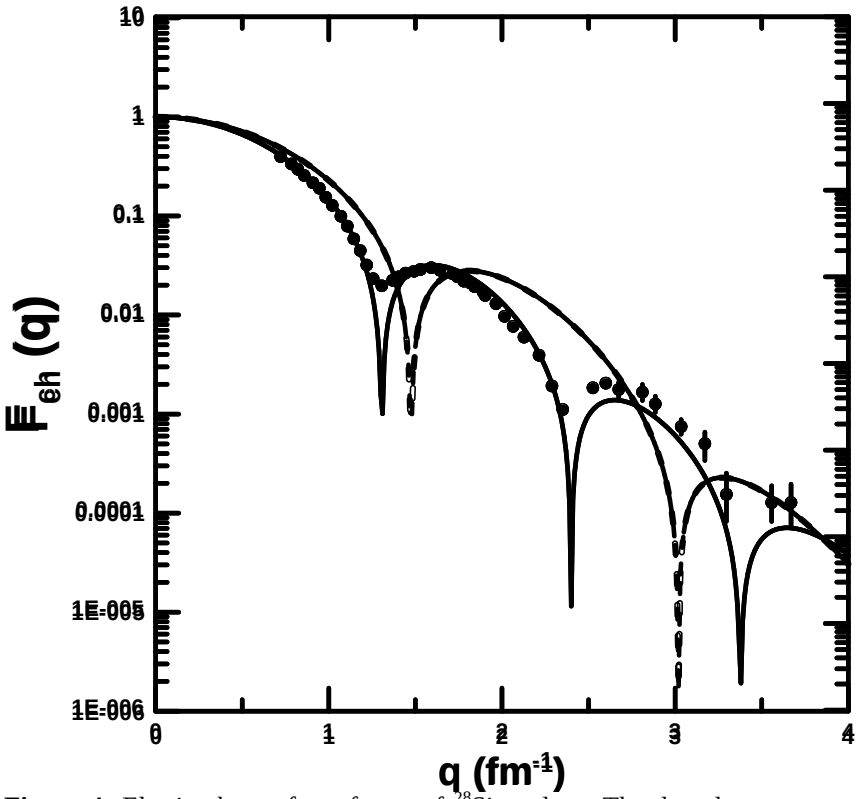

Figure 4- Elastic charge form factor of ^{28}Si nucleus. The dotted curve represents experimental data [6]. The dashed and solid curves are the calculated charge form factors calculated using SSM and MSM methods, respectively.

For ^{32}S nucleus, the HO size parameter is taken to be $b = 1.57\ fm$ to get best match with experimental charge density distribution and form factor. The occupation numbers are calculated in SSM and MSM methods and tabulated in Table -7 and -8, respectively. The calculated charge density distributions in SSM and MSM are displayed in Figure -5 also by dashed and solid curves, respectively. The results showed good agreement with experimental data. The inclusions of the effect of occupation numbers enhanced the results to become closer to the data.

In figure -6, the calculated elastic charge form factors are displayed by dashed and solid curves calculated in SSM and MSM, respectively. The result of solid curve is remarkably improved more than the result of SSM and the position of diffraction minima are well-predicted more than the result of SSM which completely fail to generate such positions.

The results of the calculated rms charge, neutron, and matter radii are tabulated in Table -9. The results of the calculated charge rms and matter radii in MSM are overestimated in comparison with experimental data, on contrary to the results of the SSM which underestimated the result in comparison with experimental data this due to the contribution coming from higher $1f_{7/2}$ and $2f_{7/2}$ subshell.

Table 7- The calculated $X_{a,a,t_z}^{J_i,J_i,0}$ for ^{32}S for neutrons and protons calculated in SSM method.

State 1	State 2	Number of protons ($n_{a,p}$) and neutrons ($n_{a,n}$)	$X_{a,a,t_z}^{J_i,J_i,0}$
$1s_{1/2}$	$1s_{1/2}$	2.0	1.414214
$1p_{3/2}$	$1p_{3/2}$	4.0	2.0
$1p_{1/2}$	$1p_{1/2}$	2.0	1.414214
$1d_{5/2}$	$1d_{5/2}$	6.0	2.449490
$1d_{3/2}$	$1d_{3/2}$	2.0	1.0

Table 8- The calculated $X_{a,a,t_z}^{J_i,J_i,0}$ for ^{32}S for neutrons and protons calculated in MSM method.

State 1	State 2	Number of protons ($n_{a,p}$) and neutrons ($n_{a,n}$)	$X_{a,a,t_z}^{J_i,J_i,0}$
$1s_{1/2}$	$1s_{1/2}$	1.5	1.060660
$1p_{3/2}$	$1p_{3/2}$	3.5	1.75000
$1p_{1/2}$	$1p_{1/2}$	1.3	0.919239
$1d_{5/2}$	$1d_{5/2}$	1.4	0.571548
$1d_{3/2}$	$1d_{3/2}$	0.0	0.0
$2s_{1/2}$	$1p_{1/2}$	0.35	0.247487
$1f_{7/2}$	$1d_{5/2}$	7.4	2.616295
$1f_{5/2}$	$1d_{3/2}$	0.0	0.0
$2p_{3/2}$	$1p_{1/2}$	0.0	0.0
$2p_{1/2}$	$1d_{5/2}$	0.0	0.0
$1g_{9/2}$	$1d_{3/2}$	0.0	0.0
$1g_{7/2}$	$1p_{1/2}$	0.0	0.0
$2d_{5/2}$	$1d_{5/2}$	0.0	0.0
$2d_{3/2}$	$1d_{3/2}$	0.0	0.0
$3s_{1/2}$	$1p_{1/2}$	0.0	0.0
$1h_{11/2}$	$1d_{5/2}$	0.0	0.0
$1h_{9/2}$	$1d_{3/2}$	0.0	0.0
$2f_{7/2}$	$1p_{1/2}$	0.55	0.194454
$2f_{5/2}$	$1d_{5/2}$	0.0	0.0

Table 9-The calculated rms charge, neutron, and matter radii of ^{32}S nucleus.

Technique	$\langle r \rangle_{ch}^{1/2}$ *fm*	Exp. $\langle r \rangle_{ch}^{1/2}$ *fm* [13]	$\langle r \rangle_{n}^{1/2}$ *fm*	$\langle r \rangle_{m}^{1/2}$ *fm*	Exp. $\langle r \rangle_{m}^{1/2}$ *fm*
SSM	3.071	3.239(30)	2.967	2.967	-
MSM	3.403		3.310	3.310	-

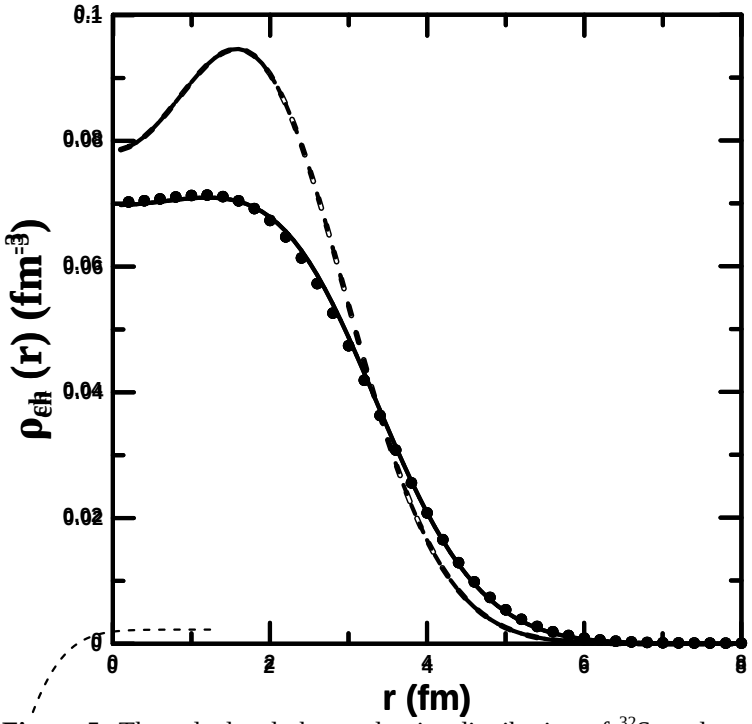

Figure 5- The calculated charge density distribution of ^{32}S nucleus. The dotted curve represents experimental data [13]. The dashed and solid curves are the calculated charge density using SSM and MSM, respectively.

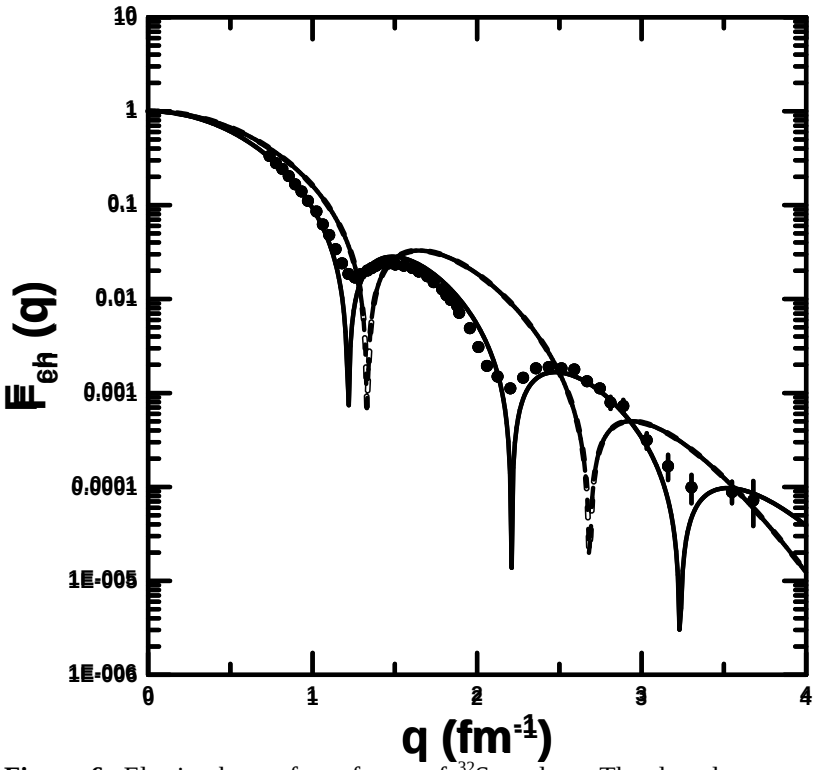

Figure 6- Elastic charge form factor of ^{32}S nucleus. The dotted curve represents experimental data [6]. The dashed and solid curves are the calculated charge form factors calculated using SSM and MSM methods, respectively.

Conclusion

The effects of occupation numbers on the ground charge density distributions, elastic form factors and root mean square (rms) radii are investigated for ^{24}Mg, ^{28}Si and ^{32}S nuclei using single-particle radial wave functions of harmonic-oscillators (HO) potential. It was concluded that the mixing configuration between nuclear shells is important and needed to make the result in agreement with experimental data. For the calculated charge density distributions, the results showed good agreement with experimental data except the overestimation to produce the density in the central region for ^{28}Si nucleus. In general, the calculations for elastic charge form factors showed good agreement to predict the positions of diffraction minima.

References

1. Bergstrom, J. C., Kowalski, S. B. and Neuhausen, R.**1982**. Elastic magnetic form factor of ^{6}Li, *Physical Review* C 25, pp: 1156-1167.
2. Hamoudi, K., Radhi, R. A., Flaiyh, G. N. and Shrrad, F. I. **2010**. The effect of two body correlations on the charge density distributions and elastic electron scattering form factors for some 2s-1d shell nuclei, *Journal of Al-Nahrain University*, 13, pp: 88-98.
3. Radhi, R. A., Ridha, A. R. and Majeed, W. Z. **2015**. Cormparison between shell model and self-consistent mean field calculations for ground charge density distributions and elastic form factors of ^{12}C and ^{16}O nuclei, *Indian Journal of physics*, 89, pp: 723-728.
4. Brain, S. W., Johnston, A., Gillespie, W. A., Lees, E. W. and Singhal, R. P. **1977**. The ground-state charge distribution of the silicon isotopes and the excited states of 28Si, 30Si, *Journal of Physics G: Nuclear Physics*, 3, pp: 821-832.
5. Wesseling, J., de Jager, C. W., Lapikás, L., de Vries, H., Fagg, L. W., Harakeh, M. N., Kalantar-Nayestanaki, N., Lindgren, R. A., Moya De Guerra, E. and Sarriguren, P.**1997**. $2s_{1/2}$ occupancies in ^{30}Si, ^{31}P, and ^{32}S, *Physical Review* C 55, pp: 2773-2786.
6. Hamoudi, K., Radhi, R. A. and Ridha, A. R. **2012**. Theoretical study of matter density distribution and elastic electron scattering form factors for the neutron– rich ^{22}C exotic nucleus. *Iraqi Journal of Physics*, 10, pp:25-34.
7. Radhi, R. A., Hamoudi, K. and Ridha, A. R. **2013**. Elastic electron scattering from unstable neutron– rich ^{19}C exotic nucleus. *Iraqi Journal of Science*, 54, pp:324-332.

8. Khalid, S. J., Anwer, A., Fadhil, I. S., Hasan, A. **2014.** Elastic and inelastic electron- nucleus scattering form factors of some light nuclei: ^{23}Na, ^{25}Mg, ^{27}Al and ^{41}Ca, *Physical Review* C 89,pp:1-9.

9. Brown, B. A., Radhi, R. and Wildenthal, B. H. **1983**. Electric quadrupole and hexadecupole nuclear excitations from the perspectives of electron scattering and modern shell-model theory, *Physics Reports*. **101**, pp: 313-358.

10. Radhi, R. A. **1983**. Calculations of elastic and inelastic electron scattering in light nuclei with shell-model wave functions, Ph.D.Thesis, Department of Physics, Michigan State University, USA.

11. Brussard, P. J. and Glademans, P. W. M. **1977**. *Shell-model Application in Nuclear Spectroscopy*, North-Holland Publishing Company, Amsterdam.

12. Elton, L. R. B. **1961**. *Nuclear Sizes*, Oxford University Press.

13. Vries, H. De, De Jager, C. W. and De Vries, C.**1987**. Nuclear charge-density-distribution parameters from elastic electron scattering, *Atomic Data and Nuclear Data Tables*, 36, pp: 495-536.

14. Ozawa, A., Suzuki, T. and Tanihata, I. **2001**. Nuclear size and related topics, *Nuclear Physics* A. **693**, pp: 32-62.